Proceedings of the ASME 2010 3rd Joint US-European Fluids Engineering Summer Meeting and 8th International Conference on Nanochannels, Microchannels, and Minichannels
FEDSM-ICNMM2010
August 1-5, 2010, Montreal, Canada

FEDSM-ICNMM2010-30043

NON-STATIONARY SIGNAL ANALYSIS OF THE VON KÁRMÁN VORTEX SHEDDING IN THE WAKE OF A FLUTTERING AIRFOIL

Amin Fereidooni*
Abhijit Sarkar
Department of Civil and Environmental Engineering
Carleton University
Ottawa, Ontario, K1S 5B6
Canada
Email: afereido@connect.carleton.ca

Dominique Poirel
Azémi Benaissa
Department of Mechanical Engineering
Royal Military College of Canada
Kingston, Ontario, K7K 7B4
Canada

Vincent Métivier
Guy Dumas
Laboratoire de Mécanique des Fluides Numérique
Université Laval
Québec city, QC, G1K 7P4
Canada

ABSTRACT

Stationary data lend themselves well to the Fourier decomposition into harmonic components. Conversely, spectral characteristics of non-stationary data vary with time, and hence do not generally admit the application of Fourier transform. In order to investigate the localized time-frequency characteristics of non-stationary data, the notions of instantaneous frequency and amplitude are invoked. These concepts are applied to the von Kármán vortex shedding observed in the wake of a self-sustained pitching airfoil. For this range of Reynolds numbers ($10^4 - 10^5$), it has been reported that at any given airspeed the shedding frequency of the vortex street varies with angle of attack (AOA), ranging from the Strouhal number St ≈ 0.6 at zero AOA and tending to St ≈ 0.1 for high AOA. For the pitching motion, which originates from a positive energy transfer from the flow to the airfoil due to negative aerodynamic damping, the von Kármán vortex shedding frequency varies with pitch angle hence with time. Hilbert transform provides a robust estimate of instantaneous frequency through the definition of analytic signals. However, Hilbert transform provides meaningful instantaneous frequency for only monocomponent signals. To overcome this difficulty, the Hilbert-Huang transform is commonly exploited. In this paper, both the Hilbert and Hilbert-Huang transforms are applied in order to capture the instantaneous vortex shedding frequency. For multicomponent signals Empirical Mode Decomposition (EMD) splits the signal to monocomponent signals, namely Intrinsic Mode Functions, through a so-called sifting process. Application of Hilbert transform to these functions produces instantaneous frequencies and amplitudes. Therefore the time-frequency-amplitude representation of the signal appears to be a promising tool for obtaining more physical insight into the time-varying vortex shedding frequency in the wake of a pitching airfoil.

1 INTRODUCTION

Time-frequency characteristics of vortex shedding in the wake of a self-sustained pitching airfoil is investigated using time-frequency analysis tools. Initially, a brief introduction to time-frequency analysis is presented. The concepts of Hilbert transform and analytic signal are reviewed and a simple example is adapted to demonstrate the performance of Hilbert transform in order to identify the local frequencies in monocompo-

*Address all correspondence to this author.

nent signals. Furthermore, Hilbert-Huang transform, a method for analysing multicomponents signals, is discussed briefly. As an illustrative example, this method is used to extract the local frequencies of the sum of two frequency modulated signals. Finally the aforementioned methods are used to explore the time-varying frequency of vortices shed in the wake of a self-sustained oscillating NACA0012 airfoil; the axis is located at 18.6% of the chord length from the leading edge. The estimated frequencies are compared to those calculated from the successive zero-crossings of the signal.

2 Hilbert Transform and Instantaneous Frequency

2.1 Definition

In the study of vibration, the notion of frequency refers to the number of cycles of oscillation per unit time [1]. This definition is well-suited for stationary data, where Fourier transform is applicable. In Fourier perspective, at least one cycle of oscillation is necessary to identify its corresponding frequency[2]. However, the spectral characteristics of non-stationary data changes with time (e.g. frequency changes with time). For non-stationary data, therefore the notion of instantaneous frequency is introduced [1, 3–5].

In 1946, Gabor introduced the definition of analytic signal through Hilbert transform [6], which offers a unique way of defining instantaneous frequency. Consider the real signal $s(t)$ where the complex analytic signal, which is defined as $z(t)$ is constructed from the real signal [7]

$$z(t) = s(t) + iH[s(t)] \tag{1}$$

where $H[.]$ refers to Hilbert transform defined as

$$H[s(t)] = \frac{1}{\pi} p \int \frac{s(t')}{t-t'} dt' \tag{2}$$

where p is the Cauchy Principal Value [4, 7]. Note that all the integrals without limits imply the integration from $-\infty$ to $+\infty$ unless otherwise stated.

It is worth mentioning that Hilbert transform is the convolution of the original signal $s(t)$ and the function $\frac{1}{t}$, which enables the identification of local properties of the signal in time [2, 7].

Consider the polar coordinate representation of the analytic signal $z(t)$ as

$$z(t) = a(t) e^{i\varphi(t)} \tag{3}$$

where

$$a(t) = \sqrt{(s(t))^2 + (H[s(t)])^2}, \tag{4}$$

$$\varphi = \arctan \frac{H[s(t)]}{s(t)}. \tag{5}$$

It can be shown that the derivative of the phase function $\varphi(t)$ is the *instantaneous frequency* [3] as discussed in the Appendix

$$\omega = \frac{d\varphi}{dt}. \tag{6}$$

In addition to the original signal $s(t)$, the need for the complex signal $z(t)$ are as follows [4]:

(1) The derivative of the phase function is defined as the instantaneous frequency. However, the phase function of the original real signal is always zero. Therefore it fails to provide any meaningful information of the frequency content of the signal. However the analytic signal constructed from the original real signal and its Hilbert transform is complex (i.e. having non-zero phase function). The derivative of this phase function provides the instantaneous frequency.

(2) The Fourier transform of a real signal is always symmetric with respect to the frequency. Thus, the mean frequency value of the signal turns out to be zero, which is again problematic. This problem can be circumvented through the complex analytic signal. In order to demonstrate this fact, let us apply the Fourier transform on the analytic function of Eq. (1), namely

$$F[z(t)] = F[s(t)] + iF[H[s(t)]]. \tag{7}$$

Eq. (7) is valid due to linear property of Fourier transform. Using the following property of Fourier transform [7]

$$F[H[s(t)]] = -i\,sgn(\omega) S(\omega) \tag{8}$$

it can easily be proved that

$$Z(\omega) = (1 + sgn(\omega)) S(\omega) = \begin{cases} 2S(\omega), & \text{if } \omega > 0 \\ 0, & \text{if } \omega < 0 \end{cases}. \tag{9}$$

Note that the spectrum of the analytic signal $z(t)$ is zero for negative frequencies and double for the positive frequencies, which maintains the energy of the analytic signal to that of the original signal. This property introduces a positive mean frequency, which is physically more plausible.

2.2 Illustrative example

In order to demonstrate the performance of Hilbert transform in identifying local frequency, the Hilbert transform is applied to the frequency modulated signal depicted in Fig. 1. The mathematical description of the signal is given by

$$s(t) = \begin{cases} \sin(2\pi(0.4t+2)t), & \text{if } 0 \le t \le 5s \\ \sin(2\pi(3)t), & \text{if } 5s < t \le 10s \end{cases}. \tag{10}$$

According to Eq. (6), the instantaneous frequency can be obtained by finding the derivative of the phase function with respect

to time, namely

$$\omega = \frac{d\varphi}{dt} = \begin{cases} 2\pi\,(0.8t+2)\,, & \text{if } 0 \le t \le 5s \\ 2\pi\,(3)\,, & \text{if } 5s < t \le 10s \end{cases}. \qquad (11)$$

The frequency of the signal changes linearly up to $5s$: it begins at $2Hz$ and ends $6Hz$ at $5s$. At this time instance, the frequency drops off sharply and becomes $3Hz$. This frequency remains constant until the end of oscillation.

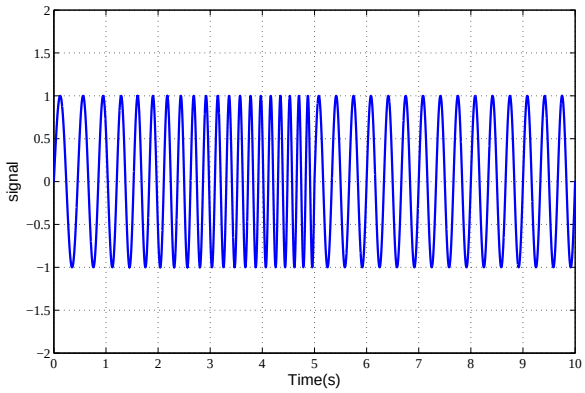

FIGURE 1. Monocomponent frequency modulated signal $s(t)$

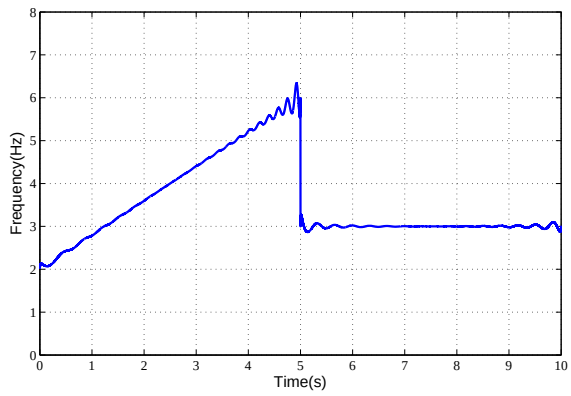

FIGURE 2. Hilbert transform of frequency modulated signal $s(t)$

The Hilbert and Fourier transforms of the signal are shown in Fig. 2 and Fig. 3 respectively. Since Hilbert transform involves convolution with time, it is able to capture the variation of frequency in time, whereas Fourier transform fails to provide such information.
Note that Hilbert transform only provides meaningful instantaneous frequency for monocomponent signals [2]. An extension of Hilbert transform, namely Hilbert-Huang transform is

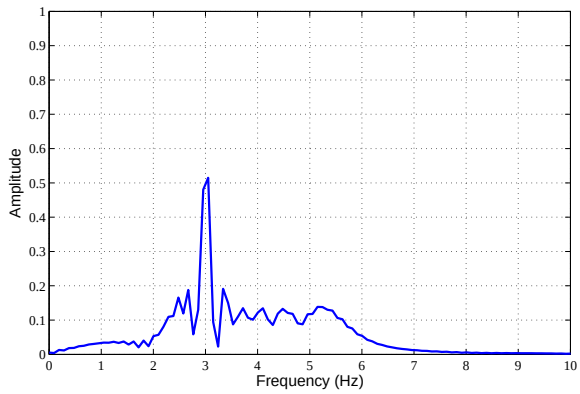

FIGURE 3. Fourier transform of frequency modulated signal $s(t)$

proposed by Huang et al.[2] to handle multicomponent non-stationary signals as discussed next.

3 Intrinsic Mode Functions

3.1 Definition

Huang et al. [2] proposed two restrictions in order to guarantee a well defined signal for applicability of Hilbert transform:
(1) The signal has to possess the same number of zero crossings and extrema.
(2) The signal has to be symmetric with respect to local zero mean.
Huang et al. [2] proposed Empirical Mode Decomposition method (EMD) that decomposes any arbitrary signal into a set of oscillatory modes that satisfies the aforementioned restrictions. These oscillatory modes are referred to as *Intrinsic Mode Functions* (IMF). EMD decomposes the signal into IMFs through a procedure called *sifting process*, which is described as following [2]:
(1) The extrema are identified first. Then upper and lower envelopes are constructed by connecting all maxima and minima respectively. The mean of the two envelopes m_1 is computed and subtracted from the original signal. The result is called h_1:

$$s(t) - m_1 = h_1. \qquad (12)$$

(2) In order to obtain a more symmetric signal, step 1 is repeated. Hence h_1 is treated as the original signal and h_{11} is obtained as

$$h_1 - m_{11} = h_{11}. \qquad (13)$$

(3) After k time repetitions of the process, the result is

$$h_{1(k-1)} - m_{1k} = h_{1k}. \qquad (14)$$

Thus the first IMF is given by

$$IMF_1 = h_{1k}. \qquad (15)$$

(4) The criterion for stopping the iteration can be expressed in terms of the standard deviation SD, computed from the two successive sifting processes, i.e.

$$SD = \sum_{t=0}^{T} \left[\frac{\left| h_{1(k-1)}(t) - h_{1k}(t) \right|^2}{h_{1(k-1)}^2(t)} \right]. \tag{16}$$

The typical limit on the value of SD can be set between 0.2 and 0.3.
(5) For the extraction of the second IMF, IMF_1 is subtracted from the original signal, namely

$$s(t) - IMF_1 = r_1. \tag{17}$$

Then the residual, r_1, is treated as the original signal and the steps 1 to 4 are applied to it. After performing the sifting process iteratively until the stopping criterion is satisfied, the second IMF is extracted.
(6) The entire process is repeated until $nIMFs$ are produced, i.e.

$$r_{i-1} - IMF_i = r_i \quad 2 < i < n. \tag{18}$$

There are two criteria to terminate the entire process:
(a) When IMF_n or residual r_n is smaller than a specified value.
(b) r_n is a monotonic function from which no IMF can be extracted.
Finally the complete decomposition process can be summarized through the following equation:

$$s(t) = \sum_{i=1}^{n} IMF_i + r_n. \tag{19}$$

3.2 Illustrative example

In order to demonstrate the application of EMD on multicomponent signals, the sum of two frequency modulated signals is considered in this section. The sum of the two complex signals $a_1(t)e^{i\varphi_1(t)}$ and $a_2(t)e^{i\varphi_2(t)}$ with time varying amplitudes and frequencies, has an instantaneous frequency given by [5]

$$\varphi'(t) = \frac{1}{2}\left(\varphi_1'(t) + \varphi_2'(t)\right) + \frac{\frac{1}{2}\left(\varphi_1'(t) - \varphi_2'(t)\right)\left(a_1^2(t) - a_2^2(t)\right)}{a^2(t)} + \frac{\left(a_1'(t)a_2(t) - a_2'(t)a_1(t)\right)\sin\left(\varphi_1(t) - \varphi_2(t)\right)}{a^2(t)} \tag{20}$$

with

$$a^2(t) = a_1^2(t) + a_2^2(t) + 2a_1(t)a_2(t)\cos\left(\varphi_1(t) - \varphi_2(t)\right). \tag{21}$$

Note that the prime symbol ($'$) implies the derivative of the function. We consider the sum of two frequency modulated signals given by

$$s(t) = \cos\left[2\pi(0.1t + 2)t\right] + 2\cos\left[2\pi(0.2t + 4)t\right]. \tag{22}$$

This signal is plotted in Fig. 4. Fig. 5 shows the Fourier transform of the signal. Evidently, the frequency band of the signal spans from $2Hz$ to $8Hz$. However the Fourier transform of the signal is not able to detect the variation of frequency in time. In order to obtain the instantaneous frequency, first the analytic signal corresponding to $s(t)$ is constructed numerically using Hilbert transform. Next the instantaneous frequency of the same signal is calculated using Eq. (20). Instantaneous frequencies obtained by these two methods show excellent agreement as evident from Fig. 6. Although Hilbert transform identifies the general trend in the temporal variation of frequency, it cannot provide any information of the individual components buried in the multicomponent signal.
Fig. 7 shows the IMFs extracted from the signal using EMD. Note that the two components are completely separated. These components are well suited for applying Hilbert transform. The frequency contents of the IMFs can be estimated from Fig. 8 and Fig. 9, which closely match:

$$\omega = \frac{d\varphi}{dt} = \begin{cases} 2\pi(0.2t + 2), & \text{IMF1} \\ 2\pi(0.4t + 4), & \text{IMF2} \end{cases}. \tag{23}$$

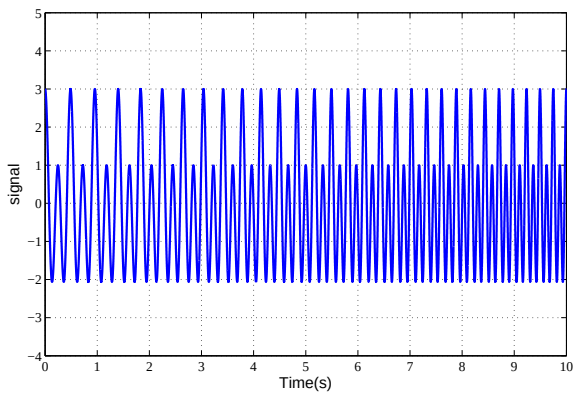

FIGURE 4. Sum of two frequency modulated signals

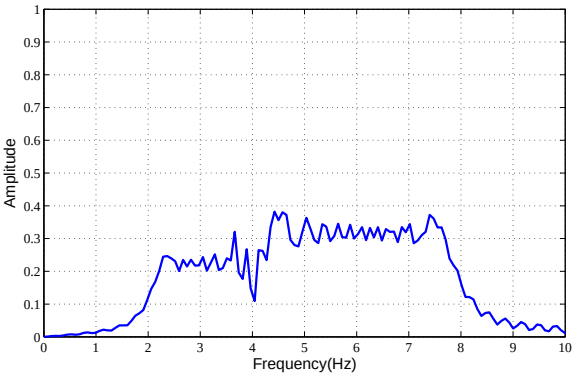

FIGURE 5. Fourier transform of $s(t)$

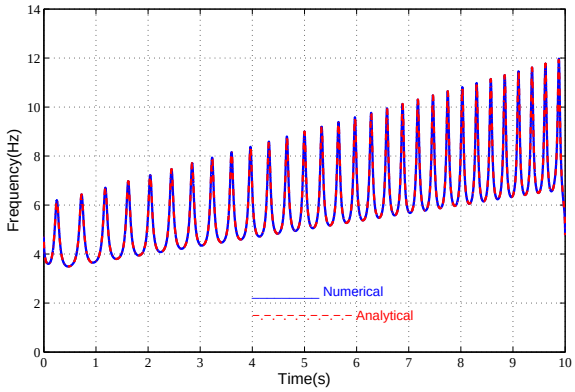

FIGURE 6. Hilbert transform of $s(t)$

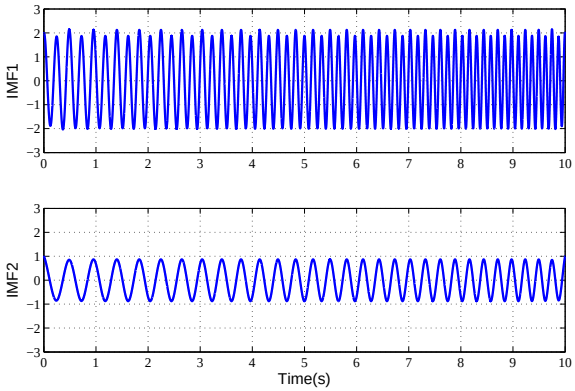

FIGURE 7. IMFs extracted from $s(t)$

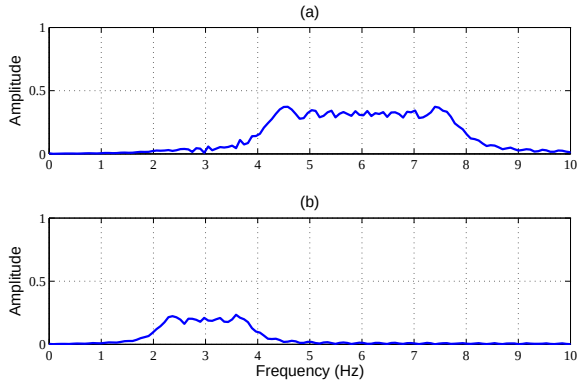

FIGURE 8. Fourier transform of the IMFs extracted from $s(t)$: (a) first IMF (b) second IMF

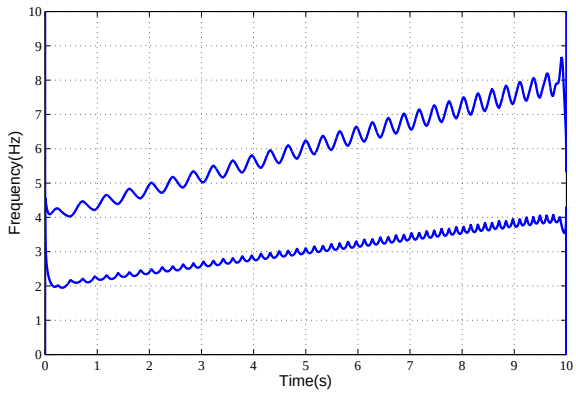

FIGURE 9. Time-frequency representation of $s(t)$

4 Vortex shedding frequency of a pitching airfoil

A rigid, but flexibly mounted, NACA0012 airfoil is oscillating freely in transitional Reynolds number and incompressible flow. Its axis of rotation is located at 18.6% chord. The phenomenon of low amplitude self-sustained pitch oscillations in this flow regime ($5.0 \times 10^4 < Re_c < 1.2 \times 10^5$) has recently been observed experimentally and numerically (See Poirel et al. [8], Poirel and Yuan [9] and Métivier et al. [10]). It has been shown that the laminar separation of the boundary layer near the trailing edge plays a critical role in sustaining the pitching oscillations. Their main features are small amplitude ($\theta < 5.5°$) and essentially simple harmonic motion whose frequency can be related to the so-called aeroelastic natural frequency, as calculated using linear thin-airfoil theory with unsteady effects based on Theordorsen's model. It is shown not to coincide with a simple von Kármán vortex shedding mechanism which occurs at frequencies two orders of magnitude higher. Accordingly, the high-frequency, shear instabilities present in the flow which leads to von Kármán vortex shedding are not crucial, nor necessary, to the maintaining mechanism of the self-sustained aeroelastic oscillations. They exist regardless if the airfoil is pitching or not. For the statically held airfoil, Huang et al. [11] showed experimentally that the shedding frequency, as characterized by the Strouhal number, $St = f_s d/U$, decreases with angle of attack and converges toward a value of $St \approx 0.1$ for angles above 20°, which is close to the classic bluff-body value of 0.2. The parameter, d, is the frontal projection that the airfoil makes with the incoming free-stream. For the NACA0012 airfoil at small angles of attack, the value of d will be very close to $0.12c$, where c is the chord length.

4.1 Numerical study

4.1.1 simulation set-up The case studied here originates from a two-dimensional aeroelastic numerical simulation performed at the Laboratoire de Mécanique des Fluides Numériques (LMFN) at Laval University. The mesh generator and flow solver used in this study are the commercial codes Gambit 2.3 and Fluent 6.3. Spatial and temporal discretizations were performed with second-order schemes for all quantities. The velocity-pressure coupling is based on a SIMPLE segregated algorithm. Unstructured meshes are used throughout this investigation. The flow is simulated based on the incompressible Unsteady Reynolds Averaged Navier-Stokes (URANS) equations under Boussinesq's assumption. The URANS simulations were run with the $SST\ k-\omega$ turbulence closure model and with the transitional flow option activated. The transitional flow option specifies a low-Reynolds-number dampening correction to the turbulent viscosity and allows for a more accurate representation of the actual flow, which is expected to exhibit an attached laminar boundary layer up to separation. This aspect of the modeling is critical since unsteady separated flows may be strongly affected by the choice of turbulence and transition models.

The elastically mounted rigid airfoil is modeled as a one degree-of-freedom in pitch, with linear structural forces balancing the aerodynamic loads. The structural equation is solved at every time-step and is then coupled with the flow solver, as illustrated in the Fig. 10. The time-step size for the calculations is $\Delta t = 10^{-5}\,s$, i.e., over 30,000 time-steps per aeroelastic oscillation ($3Hz$) and about 400 time-steps per Strouhal period due to von Kármán vortex shedding ($\approx 250Hz$). At each time-step, iterations were carried out until an RMS convergence criterion of 10^{-5} on all residuals was reached.

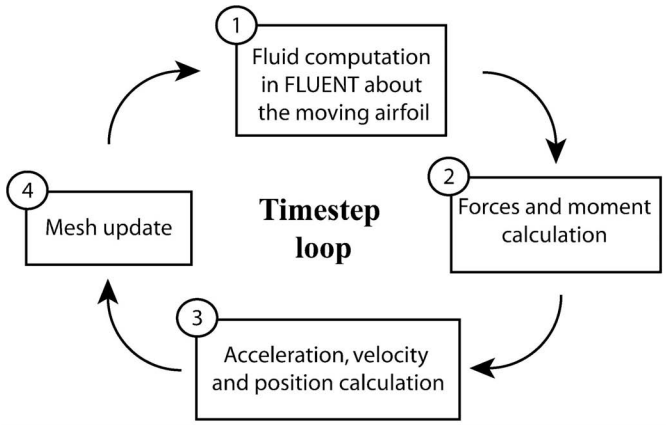

FIGURE 10. Calculation algorithm

The pitching airfoil problem is here solved in a fixed frame of reference, which thus requires moving body and moving grid capabilities. To retain second-order time accuracy in Fluent, deforming mesh and re-meshing around the rotating airfoil is avoided. Rather, a circular, non-conformal sliding interface located on a radius of two chords about the pitching axis is used. This allows taking into account the oscillating motion of the airfoil without deforming the mesh since the inner part rotates rigidly with the body while the outer part remains stationary. There is no need for time-varying boundary conditions in this case as long as only pitching oscillations are considered. The simulated airfoil is located in the center of a very large calculation domain, which extends 100 chord lengths in both directions. Constant and uniform velocity is imposed at the inlet while constant static pressure is imposed at the outlet. Far above and below the wing section, symmetry conditions are used to model slip walls. Sufficient wake and near-body resolution is used to capture accurately the vorticity gradients and to satisfy the turbulence model requirement for the first cell thickness, namely $y^+ \approx 1$ on the airfoil surface over the whole cycle.

In comparison with the experimental data, these aeroelastic simulations are found to produce reasonably accurate self-sustained pitching oscillations (LCO), with a good match in both amplitude and frequency, as well as for the wake vortex shedding frequency. Note that preliminary tests with turbulence modeling without low-Re number correction (i.e. Sparlat-Allmaras in Fluent) did not predict any LCOs. This brings support to the notion that boundary layer separation must occur on the $\theta = 0°$

airfoil configuration for any oscillation to kick in. Artificially robust boundary layers in a URANS model or tripped boundary layers in an actual laboratory set-up concur on that point. Fig. 11 shows the pitch motion as well as vertical and horizontal velocity fluctuations in the wake measured at one chord length behind the trailing edge. The free-stream velocity is $U = 6m/s$, which corresponds to a Reynolds number of $Re_c = 6.4 \times 10^4$. It is reported by Huang et al. [11] that for a static airfoil at low angle of attack $(< 8^\circ)$ and chord Reynolds number of 64000, the flow regime becomes either subcritical or transitional. It is also reported that in the subcritical regime, the periodic and smooth structure of vortex shedding as observed in the laminar regime becomes superimposed by turbulent fluctuations. The structure of vortex shedding becomes even more irregular in the case of transitional mode of flow. This irregular structure of the shed vortices in the wake can be noticed in Fig. 11.

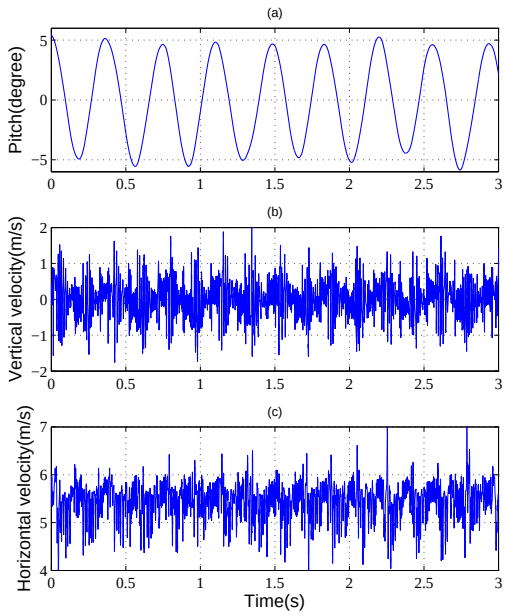

FIGURE 11. (a) Pitch motion (b) Vertical velocity at one chord length behind the trailing edge (c) Horizontal velocity at one chord length behind the trailing edge

4.1.2 Analysis The instantaneous frequency shed in the wake of the pitching airfoil is analysed using the methods described in previous sections. The pitching motion is a harmonic function with the fundamental frequency of $2.67Hz$. The velocity measurements consist of two parts: a low frequency component corresponding to the pitching motion of the airfoil and high frequency components related to the vortices shed at the trailing edge. The frequencies of these two parts are shown in Fig. 12, which illustrates the Fourier transform of the pitch motion, vertical and horizontal velocities. The low frequency component of vertical velocity has the same frequency as the pitching motion i.e. $2.67Hz$ whereas for the horizontal velocity, this frequency is double as expected.

In order to study the frequency of vortex shedding, the analysis is focused on the frequencies between $20Hz$ and $300Hz$. Thus, the frequency components outside of this range are removed using a Fourier based filter. The time and frequency results are shown in Fig. 13 and Fig. 14 respectively. Note that the vortex shedding pattern is non-periodic and turbulent-like. To obtain the instantaneous frequency of vortex shedding, the velocity responses corresponding to one full cycle of pitch motion i.e. between $0.2977s$ and $0.6863s$, is chosen for the analysis as shown in Fig. 15. Note that the pitch motions are also plotted in these figures: the pitch motion represented by the solid line shows the angular displacement of the airfoil at the same time that the velocity is obtained, whereas the dashed line represents the pitch motion at the time the vortices are shed at the trailing edge. It is worth to mention that the time lag between the two pitch motions represents the time it takes for the vortices to travel from the trailing edge to the one chord length behind the trailing edge where the velocities are obtained $(\Delta\tau = c/\bar{U}_{wake})$.

Applying the EMD procedure, the IMFs are extracted for vertical and horizontal velocities. The first five IMFs of the vertical response and their frequency contents are shown in Fig. 16 and Fig. 17 respectively. As shown in these figures, the energy of the signal is concentrated in more than one IMFs. Therefore, it can be concluded that the signal is multicomponent. Fig. 18 and Fig. 19 show the first five IMFs extracted from the horizontal velocity represented in time and frequency respectively. Fig. 17 and Fig. 19 reveal that each IMF is a narrow banded signal that has higher frequency components comparing with its successive IMF.

The instantaneous frequency of vortex shedding obtained from the vertical velocity is estimated using Hilbert transform and is shown in Fig. 20. This instantaneous frequency is also compared with the conventional frequencies calculated from zero crossings. The time lapse between two zero crossings is considered as half of the period of oscillation. These two curves illustrate the same trend in the variation of frequency except where the Hilbert transform shows drastic downshift of instantaneous frequency. These negative frequencies are not physically meaningful. In order to alleviate this difficulty, Hilbert transform should be applied on the monocomponent signals. The extracted IMFs are used to provide more insight into the shedding frequency variation. The instantaneous frequency of the first two IMFs, which contain most of the energy of the signal, are also plotted in Fig. 20. As evident from the figure, both IMFs show positive frequency contents. However the physical interpretation of these IMFs need further investigation. Fig. 21 shows the variation of frequency with angle of attack. Note that the frequency fluctuates between $50Hz$ to $500Hz$ where the first IMF exhibits higher frequency content

comparing to the second IMF. It should be mentioned that no general trend in frequency variation can be observed considering only one cycle of pitch motion. The variation of frequency with time and angle of attack for horizontal velocity are illustrated in Fig. 22 and Fig. 23 respectively.

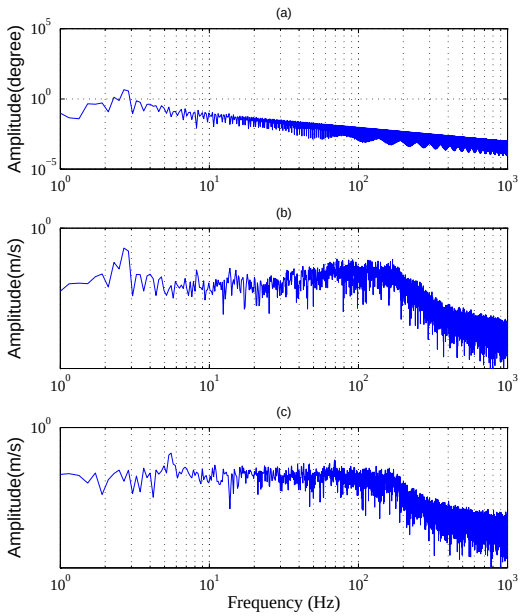

FIGURE 12. Fourier based frequency contents of: (a) pitch motion (b) vertical velocity (c) horizontal velocity

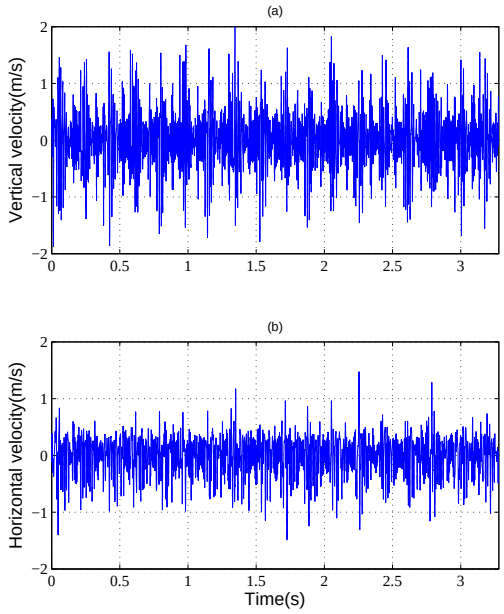

FIGURE 13. Filtered velocities: (a) vertical (b) horizontal

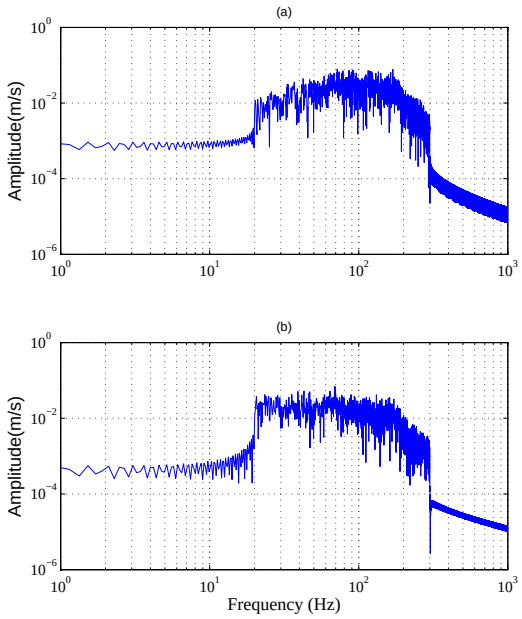

FIGURE 14. Fourier based frequency content of the filtered velocities: (a) vertical (b) horizontal

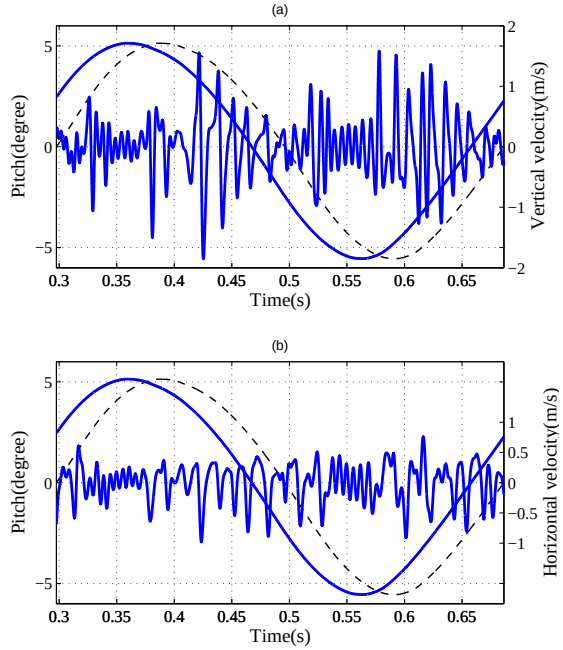

FIGURE 15. Velocity responses between $0.2977s$ and $0.6863s$: (a) vertical (b) horizontal; pitch motion: dashed line $(\theta(t))$, solid line $(\theta(t-\Delta\tau))$

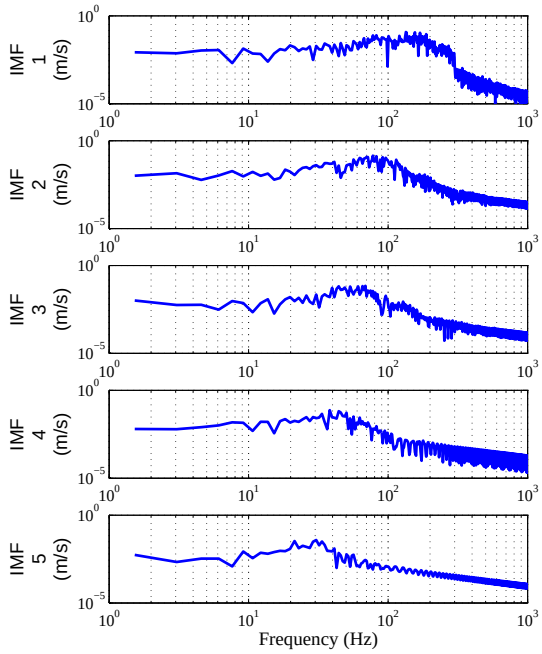

FIGURE 17. Fourier transform of the extracted IMFs: vertical velocity

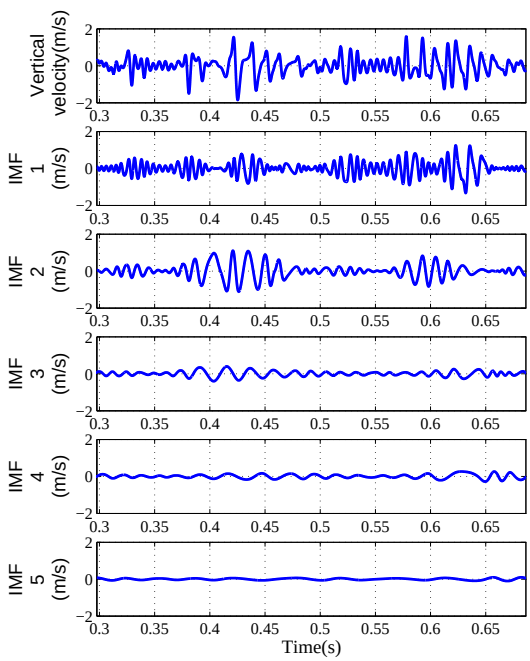

FIGURE 16. IMFs extracted from vertical velocity response between $0.2977s$ to $0.6863s$

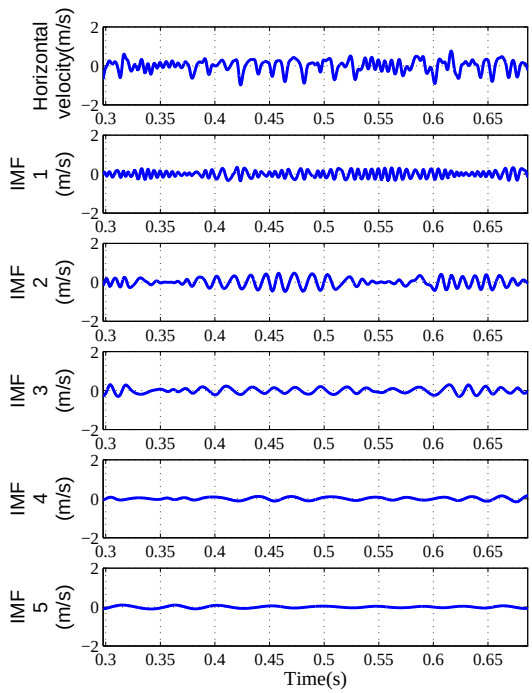

FIGURE 18. IMFs extracted from horizontal velocity response between $0.2977s$ to $0.6863s$

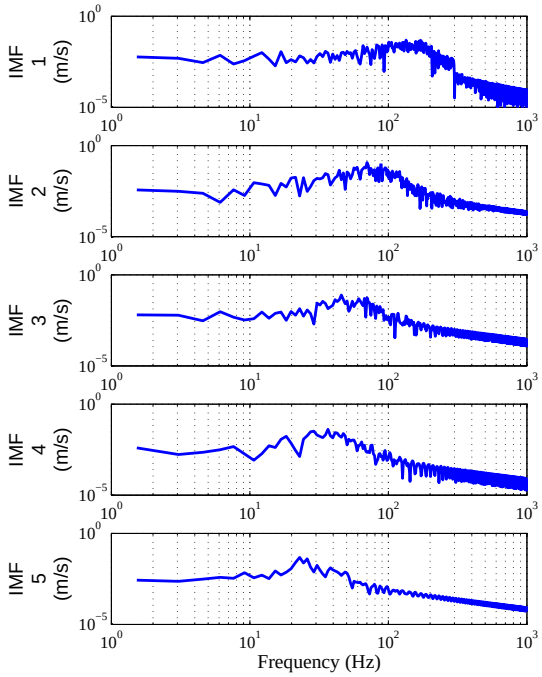

FIGURE 19. Fourier transform of the extracted IMFs: horizontal velocity

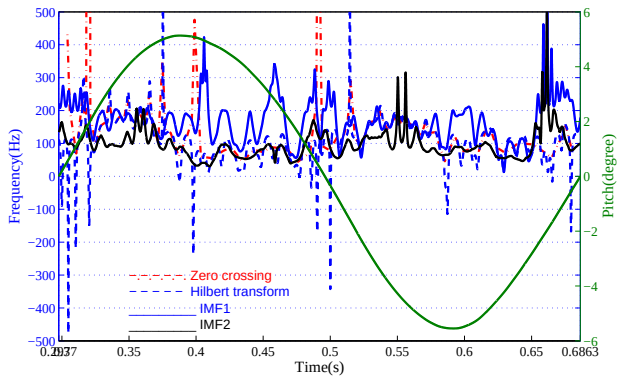

FIGURE 20. Time-frequency representation of vortex shedding at one chord length behind the trailing edge: vertical velocity

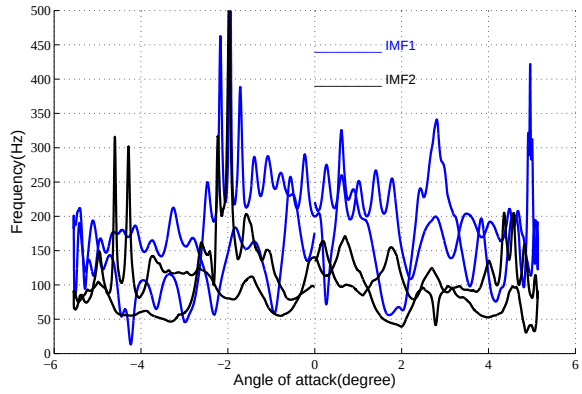

FIGURE 21. Frequency vs. angle of attack: vertical velocity

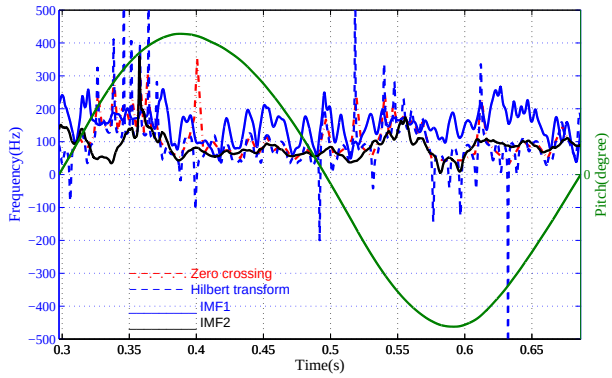

FIGURE 22. Time-frequency representation of vortex shedding at one chord length behind the trailing edge: horizontal velocity

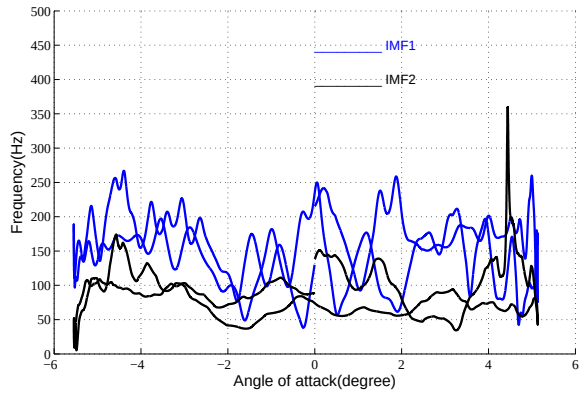

FIGURE 23. Frequency vs. angle of attack: horizontal velocity

4.2 Experimental study

4.2.1 Aeroelastic apparatus The apparatus is a two-degree-of-freedom system, composed of a rigid wing moving in translation (plunge - h) and in rotation (pitch - θ), as shown in Fig. 24. Note that the grid shown in the figure is used to artificially generate free-stream turbulence; it is not used in this work. The wing span is $s = 0.61m$ and its chord is $c = 0.156m$, thus, giving an aspect ratio of $AR = 3.9$. End plates are installed to minimize 3D effects. The gap between the wing tips and end plates is $7mm$, which is equivalent to 1% of the span. The wing and the end plates result in a solid blockage ratio of 5%. The wing is installed vertically in the test section of the wind tunnel to isolate its motion from the effect of gravity. Both the pitch and plunge dynamics are measured with rotary potentiometers and are recorded via a National Instruments PCI-6034E A/D card using a LabVIEW based data acquisition system in which the sampling rate is set at $5kHz$. In this work, the motion is restricted to pitch alone, with plunge motion held fixed.

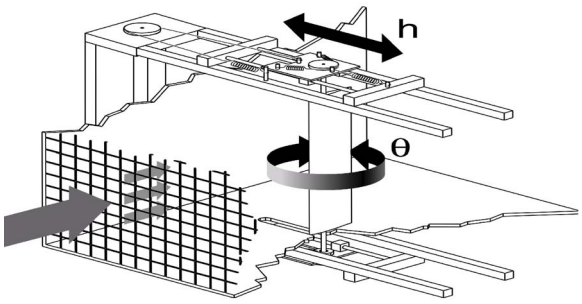

FIGURE 24. Schematic of aeroelastic rig (turbulence-generating grid not used in this work)

4.2.2 Wind tunnel facility The experiments are performed in the RMC wind tunnel. It is a closed circuit low speed tunnel powered by a $75kW$ three-phase motor. The flow velocity ranges from 4 to $60m/s$, and is controlled by varying the fan speed. These velocities result in possible chord Reynolds number (Re_c) between $40,000$ and $630,000$. The test section measures $0.76m$ by $1.08m$. The free-stream velocity is measured with a pitot-static tube located at the entrance of the test section and linked to a manometer. The flow temperature is also recorded with a thermocouple placed at the exit of the test section. Unsteady flow measurements are obtained with a hot-wire anemometer and an X-wire probe. The probe is mounted to measure the longitudinal (x) and normal (y) components of the velocity, u and v respectively. In this work, the probe is located at a distance of one chord aft of the trailing edge, and aligned with the airfoil when at $0°$ pitch angle. Data acquisition is conducted using DISA-56C17 CTA bridges and DISA-56N20 signal conditioning units. The data is sent through a high pass filter set at $1Hz$ and a low pass filter at $10kHz$. For the range of airspeeds considered in this work, a maximum turbulence intensity level $(Tu = u'_{rms}/U)$ of no more than 0.15% exists. The pitch angle and the wake velocity components, which are measured simultaneously, are shown in Fig. 25. The free-stream velocity is $U = 7.2m/s$ and the chord Reynolds number is $Re_c = 7.5 \times 10^4$. As evident from Fig. 25, the wake pattern is highly fluctuating. In addition to measurement noise, this phenomenon is due to two physical sources: relatively high velocity (high Reynolds number) that causes subcritical and transitional flow regime and the mixing of vortex structures due to unsteady effect in the aeroelastic system.

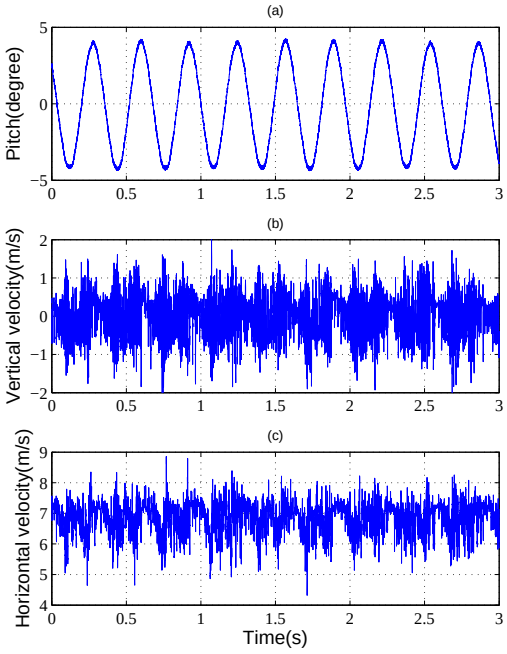

FIGURE 25. Raw measurements (a) pitch motion (b) vertical velocity at one chord length behind the trailing edge (c) horizontal velocity at one chord length behind the trailing edge

4.2.3 Analysis In this section the vortex shedding frequency in the wake of a self-sustained oscillating NACA0012 airfoil from laboratory experiment is investigated. The vortex shedding frequency of a pitching airfoil at relatively low Reynolds number $(Re_c = 27000)$ and small angle of attack $(< 3°)$ is reported by Jung et al. [12]. In this regime, the flow is laminar and the vortex shedding structure is periodic and smooth. Hence it is shown by Jung et al. [12] that the Hilbert transform provides meaningful estimation of instantaneous frequency. However due to the more complex structure of vortex shedding at higher Reynolds number $(Re_c = 75000)$, the analysis is more difficult in the current investigation.
The procedure followed in the previous section for the analysis

of the numerical data is applied to the experimental data presented in this section. Fig. 26 shows the frequency contents of the pitch motion and velocity responses using a Fourier analysis. Note that the pitch motion has a fundamental frequency of $3.1Hz$ and some superharmonics. Note that the pitch measurements captured by the the rotary potentiometer are not valid for the frequencies above $30Hz$. The velocity measurements in the wake consists of two parts: the first part includes the input frequency and its multiples that constitute the frequency content of LCO, and the second part relates to the frequency content of the vortex shedding. As shown in this figure, the frequency band of vortex shedding or more generally the wake lies in a range of $20Hz$ to $400Hz$. Therefore the frequency components outside of this range are removed from the velocity responses. Fig. 27 and Fig. 28 show these filtered responses in time and frequency domains respectively.

In order to investigate the vortex shedding frequency, the analysis is focused on the velocity responses that correspond to one cycle of pitch motion. These velocities are plotted in Fig. 29. Similar to the case of numerically simulated data, the pitch motions are also plotted in this figure: the solid line represents the pitch motion measured at the same time as the velocity is captured, and the dashed line is the lagged pitch motion at the time the vortices left the trailing edge. It should be mentioned that this time is calculated by dividing the one chord length (the distance between the trailing edge and measurement location) by the mean horizontal velocity at the wake.

The first five IMFs obtained from vertical velocity and their Fourier transform are plotted in Fig. 30 and Fig. 31 respectively. Fig. 32 and Fig. 33 show the same quantities for horizontal velocity. Again similar to the numerically simulated data, five IMFs with significant amplitude are identified. This fact reveals that the response is multicomponent and application of Hilbert transform does not lead to meaningful values of instantaneous frequency, as shown in Fig. 34 and Fig. 36 for vertical and horizontal velocity respectively. The instantaneous frequencies obtained by the zero crossing method are also plotted in these figures. The drastic increase of the estimated frequencies at some instances illustrates the failure of this Fourier based method in providing physical frequency content of the dynamical system. However using first and second IMFs, positive instantaneous frequencies that are physically more acceptable are obtained (see Fig. 34 and Fig. 36). The variation of these frequencies with angle of attack is also plotted in Fig. 35 for the vertical velocity. In order to correlate the vortex shedding frequency with the angle of attack and boundary layer conditions, perhaps more than one cycle of pitch motion seems to be necessary for the signal processing, but not carried out in this investigation.

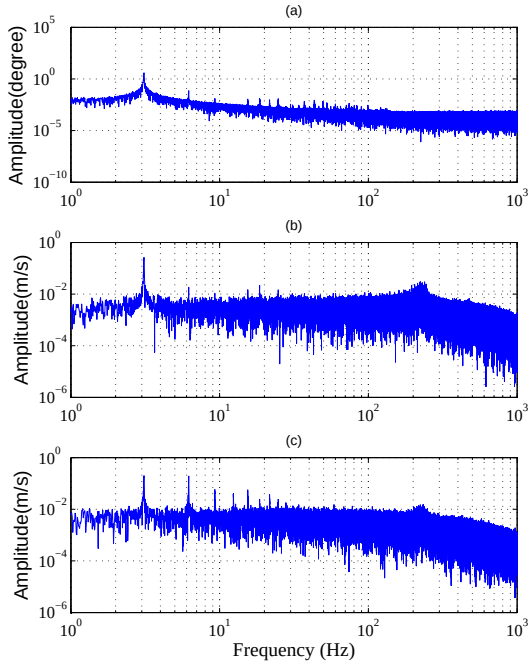

FIGURE 26. Fourier based frequency contents of: (a) pitch motion (b) vertical velocity (c) horizontal velocity

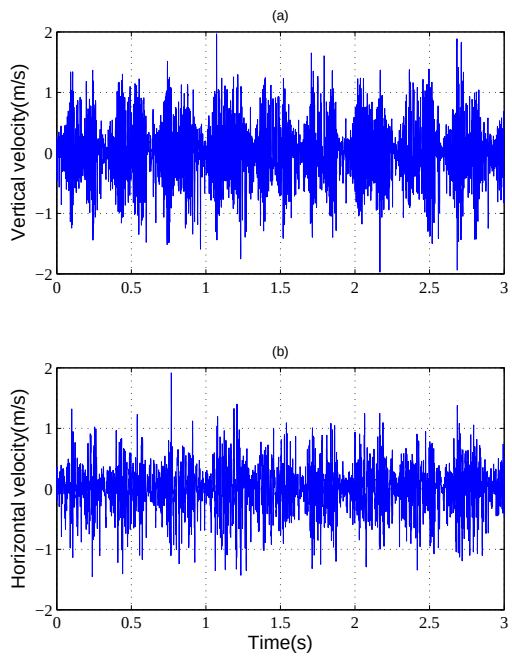

FIGURE 27. Filtered measurements: (a) vertical velocity (b) horizontal velocity

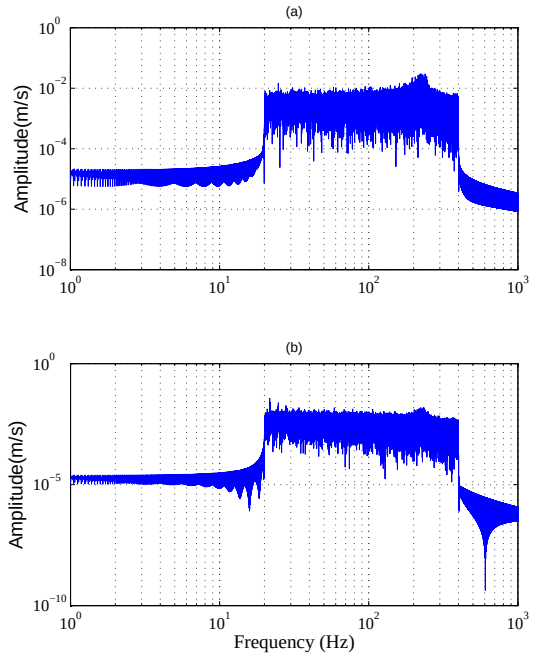

FIGURE 28. Fourier based frequency content of the filtered measurements: (a) vertical velocity (b) horizontal velocity

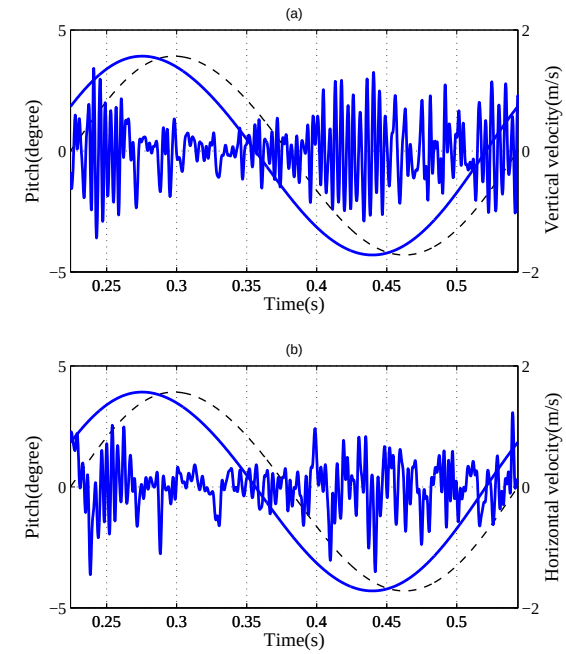

FIGURE 29. Velocity responses between $0.2242s$ and $0.5436s$: (a) vertical (b) horizontal; pitch motion: dashed line $(\theta(t))$, solid line $(\theta(t-\Delta\tau))$

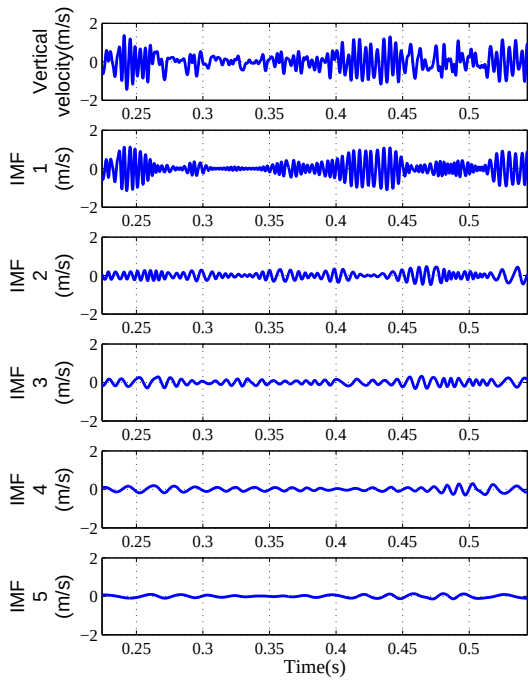

FIGURE 30. IMFs extracted from vertical velocity response between $0.2242s$ and $0.5436s$

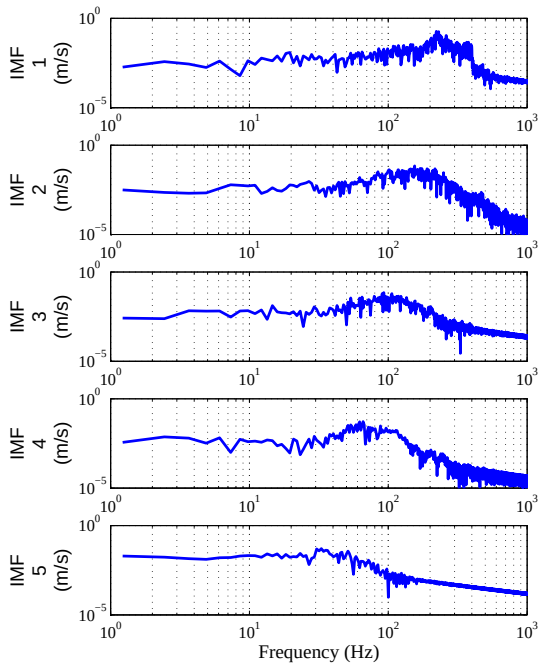

FIGURE 31. Fourier transform of the extracted IMFs: vertical velocity

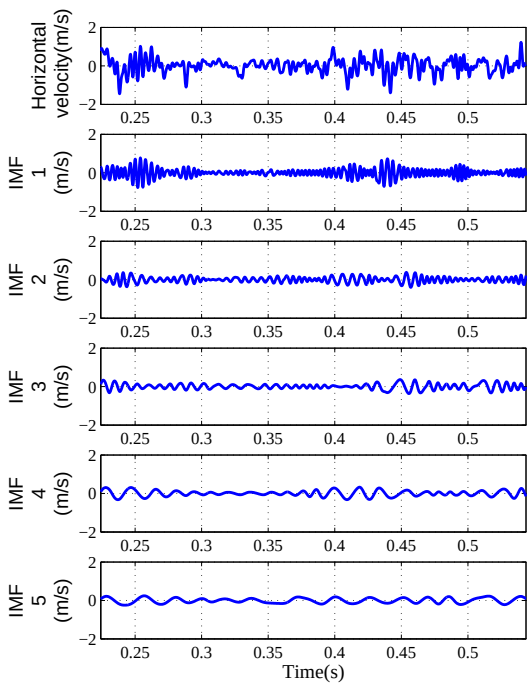

FIGURE 32. IMFs extracted from horizontal velocity response between 0.2242s and 0.5436s

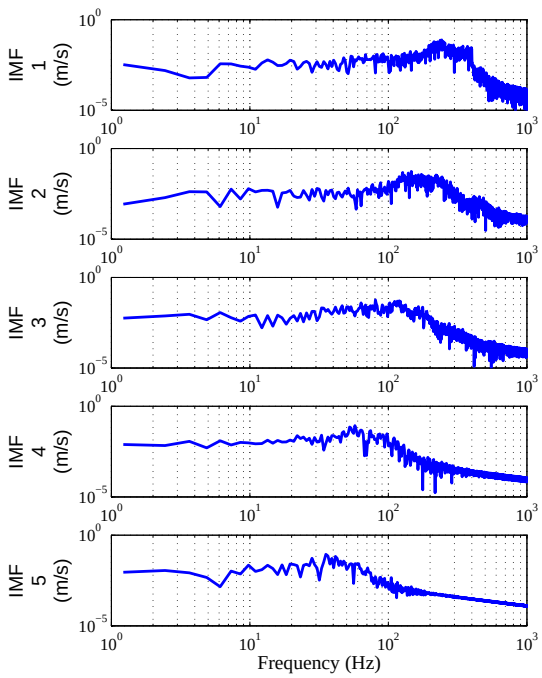

FIGURE 33. Fourier transform of the extracted IMFs: horizontal velocity

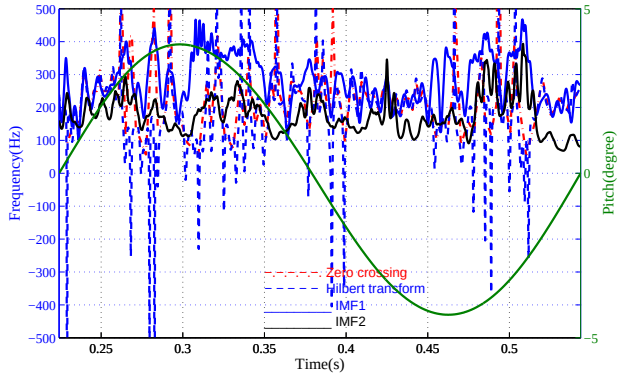

FIGURE 34. Time-frequency representation of vortex shedding at one chord length behind the trailing edge: vertical velocity

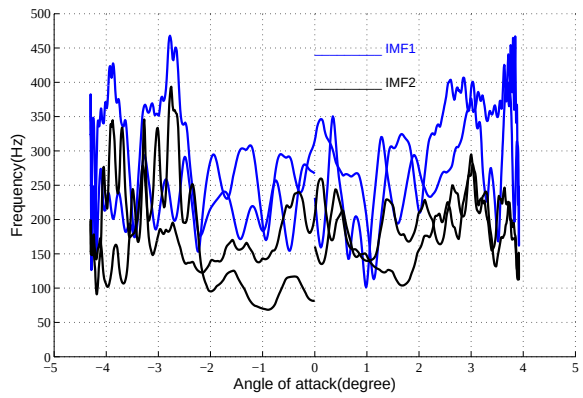

FIGURE 35. Frequency vs. angle of attack: vertical velocity

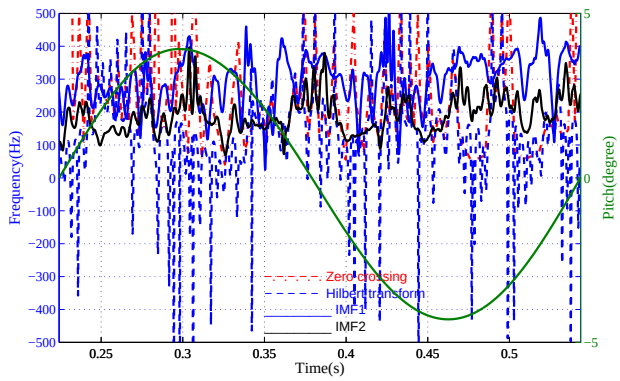

FIGURE 36. Time-frequency representation of vortex shedding at one chord length behind the trailing edge: horizontal velocity

5 CONCLUSION

Hilbert transform based non-stationary signal processing methods are applied for the estimation of vortex shedding frequency in the wake of a self-sustained oscillating NACA0012 airfoil. Since the energy of the signal is concentrated in more than one IMF, it can be concluded that the specific signals investigated here numerically and experimentally, are multicomponent in nature. The frequencies obtained using Hilbert transform demonstrate some non-physical downshifts that make the frequencies negative. These frequencies are also compared with the conventional definition of frequency defined by zero crossing rate. The estimated frequencies by zero crossing rate show some drastic increase of frequencies that reveal the difficulty of both methods in estimating the instantaneous frequencies. On the other hand, applying Hilbert transform on IMFs, leads to positive frequencies that are physically meaningful. However further investigation are required in order to relate the extracted IMFs to the physics of the dynamical system.

ACKNOWLEDGMENTS

The second author acknowledges the support of the Canadian Department of National Defense and the Natural Sciences and Engineering Research Council of Canada. The third author acknowledges the support of a Discovery Grant from Natural Sciences and Engineering Research Council of Canada and the Canada Research Chair Program.

REFERENCES

[1] Boashash, B., 1992. "Estimating and interpreting the instantaneous frequency of a signal-part 1: Fundamentals.". *Proc. of IEEE,* ***80***(4), pp. 520–538.

[2] Huang, N. E., Shen, Z., Long, S., Wu, M., Shih, H., Zheng, Q., Yen, N.-C., Tung, C., and Liu, H., 1998. "The empirical mode decomposition and the hilbert spectrum for nonlinear and non-stationary time series analysis". *Proc. Royal Society London A,* ***545***, pp. 903–995.

[3] Cohen, L., 1989. "Time-frequency distributions". *Proc. IEEE,* ***77***, pp. 941–981.

[4] Cohen, L., ed., 1995. *Time-frequency analysis*. Englewood Cliffs, NJ: Prentice-Hall.

[5] Loughlin, P., and Tacer, B., 1997. "Instantaneous frequency and the conditional mean frequency of a signal". *Signal Processing,* ***60***, pp. 153–162.

[6] Gabor, D., 1946. "Theory of communication". *J. IEE(London),* ***93***, pp. 429–457.

[7] Bendat, J., and Piersol, A., 1986. *Random Data: Analysis and Measurement Procedures*. Wiley, New York.

[8] Poirel, D., Harris, Y., and Benaissa, A., 2008. "Self-sustained aeroelastic oscillation of a naca0012 airfoil at low-to-moderate reynolds numbers". *Journal of Fluids and Structures,* ***24***(5), pp. 700–719.

[9] Poirel, D., and Yuan, W., 2008. "Aerodynamic moment of self-sustained, small amplitude, oscillations of an airfoil at re_c = 77000". In Proceedings of the 26th AIAA Applied Aerodynamics Conference, Honolulu, Hawaii, USA.

[10] Métivier, V., Dumas, G., and Poirel, D., 2009. "Aeroelastic dynamics of a naca 0012 airfoil at transitional reynolds numbers". In 39th AIAA Fluid Dynamics Conference, San Antonio, Texas, USA.

[11] Huang, R.-F., and Lin, C., 1995. "Vortex shedding and shear-layer instability of wing at low reynolds numbers". *AIAA Journal,* ***33***(8), pp. 1398–1403.

[12] Jung, Y., and Park, S., 2005. "Vortex-shedding characteristics in the wake of an oscillating airfoil at low reynolds number". *Journal of Fluids and Structures,* ***20***, pp. 451–464.

APPENDIX

This Appendix closely follows Cohen [3].
Time-frequency distributions for the signal $z(t)$ can generally be expressed by the following equation

$$P(t,\omega) = \frac{1}{4\pi^2}\int\int\int e^{-i\theta t - i\tau\omega + i\tau u}\phi(\theta,\tau) Z^*\left(u+\frac{1}{2}\theta\right) Z\left(u-\frac{1}{2}\theta\right) du\, d\tau\, d\theta \tag{24}$$

where $\phi(\theta,\tau)$ is called the kernel and Z is the Fourier spectrum of $z(t)$. The local or mean conditional frequency at a particular time is given by

$$\langle\omega\rangle_t = \frac{1}{P_1(t)}\int \omega P(t,\omega) d\omega \tag{25}$$

where $P_1(t)$ is the the density in time,

$$P_1(t) = \int P(t,\omega) d\omega \tag{26}$$

and is equal to $\left|z(t)^2\right|$. Substituting the polar coordinate representation of the analytic signal $z(t) = a(t)e^{\varphi(t)}$ into Eq. (25) leads to

$$\langle\omega\rangle_t A^2(t) = \frac{1}{2\pi}\int\int A^2(t)\left[\phi(\theta,0)\varphi'(u) - i\frac{\partial\phi(\theta,\tau)}{\partial\tau}|_{\tau=0}\right] e^{i\theta(u-t)} d\theta\, du \tag{27}$$

For the product kernel i.e.$\phi(\theta,\tau) = \phi(\theta\tau)$, Eq. (27) becomes

$$\langle\omega\rangle_t A^2(t) = \phi(0)A^2(t)\varphi'(t) + 2\phi'(0)A(t)A'(t) \tag{28}$$

If it is assumed that $\phi(0) = 1$ and $\phi'(0) = 0$, Eq. (28) leads to the following important result

$$\langle\omega\rangle_t = \varphi'(t) \tag{29}$$

Eq. (29) shows that at any particular time, the local frequency can be obtained as the derivative of the phase function of the analytic signal constructed from the original real signal.

